Available online at www.sciencedirect.com
ScienceDirect
Cement and Concrete Research 37 (2007) 1666–1673
Cement and Concrete Research

Characterization and simulation of microstructure and properties of EPS lightweight concrete

D. Bouvard [a,*], J.M. Chaix [a], R. Dendievel [a], A. Fazekas [b], J.M. Létang [c], G. Peix [c], D. Quenard [d]

[a] Laboratoire SIMAP, INPGrenoble/CNRS/UJF, BP 46, 38402 Saint Martin d'Hères Cedex, France
[b] Laboratoire MATEIS, INSA-Lyon/CNRS, 69621 Villeurbanne Cedex, France
[c] Laboratoire CNDRI, INSA-Lyon, 69621 Villeurbanne Cedex, France
[d] CSTB, 24 rue Joseph Fourier, 38400 Saint Martin d'Hères, France

Received 19 January 2007; accepted 21 August 2007

Abstract

EPS concretes are composed of high performance cement mixed with millimetre-size expanded polystyrene spheres. They exhibit *a priori* contradictory thermal and mechanical features that are suitable for the construction industry. This paper aims at characterizing the microstructure and the properties of EPS concretes and investigating the possibility of predicting these properties through various modelling approaches. It is shown that EPS concretes cannot compete against classical autoclaved cellular concrete in terms of properties but it is however a practical material whose properties can easily be tuned by changing its composition. Modelling should be a useful support for predicting the relation between properties and composition.

Keywords: Light concrete; Microstructure; Compressive strength; Thermal properties; Modeling

1. Introduction

Lightweight concrete can be obtained by replacing totally or partially standard aggregate by low weight and preferentially low cost components. The interest is of course to decrease the volume of load-bearing elements but also to get better thermal properties with regard to conventional concrete. This last point is especially relevant with regard to the new European regulations that aim at reducing energy consumption in buildings. Achieving both the thermal insulation and the bearing structure with a unique material is indeed an attractive idea, which would allow in particular the suppression of thermal bridges present in conventional buildings techniques. The difficulty is to find a material that fulfils *a priori* contradictory requirements: a low thermal conductivity- for which the presence of void is suitable – and a high mechanical strength – for which matter instead of void is needed.

Among the various types of lightweight concretes that have been proposed in the past decades, those obtained by mixing high performance cement with millimetre-size expanded polystyrene (EPS) spheres [1,2] are particularly interesting for various reasons. First, it is expected that structural elements in EPS concrete can be fabricated on construction site. This is an important advantage with respect to other materials such as autoclaved cellular concrete, whose fabrication process is rather complex. In addition, it is possible to tailor the properties of EPS concrete by varying material parameters such as EPS sphere size and volume fraction. For this purpose an accurate knowledge of the relationship between the composition and the properties of this material is required. Such relationship can be deduced from series of experiments, but modelling is expected to be fruitful to provide general trends and reduce the experimental effort.

The literature in the field of EPS concrete is mostly devoted to characterizing the mechanical properties of these materials [3–6]. It has been shown that these properties can be significantly improved by adding steel fibres or silica fume in

* Corresponding author.
E-mail address: didier.bouvard@inpg.fr (D. Bouvard).

0008-8846/$ - see front matter © 2007 Elsevier Ltd. All rights reserved.
doi:10.1016/j.cemconres.2007.08.028

the concrete matrix [3–5] or by decreasing EPS sphere size [6]. Miled et al. [7] developed a 2D numerical model to analyse such size effects. In most cases, EPS concretes with densities higher than 1000 kg/m^3 have been investigated, since a compressive strength higher than 10 MPa was searched for. Bonacina et al. [8] proposed an analytical heat transfer model to predict the thermal properties of light concretes and validated it from experimental data obtained with EPS concretes with low density, around 450 kg/m^3, which showed a thermal conductivity about 0.14 W m^{-1} K^{-1}. As far as we know, there has not been any paper analysing both mechanical and thermal features of EPS concrete with a view to seeking a compromise composition. It should however be noted that thermal and mechanical tests have been performed with concrete containing porous ceramic spheres (usually called cenospheres) [9]. For the lowest considered density, 1100 kg/m^3, Blanco et al. found a compressive strength of 5 MPa and a thermal conductivity of 0.4 W m^{-1} K^{-1}.

The aim of this paper is thus to characterize thermal and mechanical properties of EPS concrete and to investigate the possibility of predicting these properties through modelling approaches. EPS concretes with different compositions have been fabricated. Their microstructure has been analysed in 3D by X-ray tomography and their thermal and mechanical properties have been measured. The thermal behaviour has next been modelled with a classical scheme of homogenisation for two phase materials, which appeared to be sufficient. A more complex model originally developed for metal foams is proposed to calculate the mechanical resistance. This model required the creation of numerical microstructures, which have been obtained from random arrays of spheres and compared to tomography images of the real microstructures. Finally, from the comparison between experimental data and model prediction, the interest of modelling for optimising EPS concrete composition is discussed.

2. Materials

The materials investigated in this paper are EPS concretes. They are composites constituted of two phases, a high performance cement of compressive strength around 150 MPa and EPS spheres. The spheres are mixed directly with the matrix during the fabrication process. Different materials have been fabricated by changing the mass fraction and the size distribution of the spheres. Two size distributions of spheres have been used. A close distribution with spheres with a diameter between 0.75 and 1.1 mm (average 1 mm) and a two-size distribution with 30 vol.% of spheres with a diameter between 0.75 and 1.1 mm and 70 vol.% with a diameter between 1.5 and 2.6 mm (average 2.2 mm). This second structure is supposed to result in denser sphere packing density and thus in lower concrete density. By introducing more or less porosity in the blend, eight concretes with various mass densities between 432 and 961 kg/m^3 have been obtained, which correspond to cement volume fractions between 0.204 and 0.415. Specimens of dimension $4\times4\times16$ cm^3 have been fabricated for thermal characterization and cubes of 4 cm edge have been fabricated for mechanical testing and microstructural observation following EN 12390-2 European Norm standard.

3. 3D imaging of microstructure

X-ray tomography allows the non invasive evaluation of materials for a large set of purposes [10], including concrete [11]. The usual technique, named transmission tomography or attenuation tomography, is based on the measurement of X-ray attenuation along a set of directions throughout the evaluated object. For that purpose a set of radiographic images, named projections, are captured, corresponding to different directions of irradiation. At a given X-ray energy and for every sensitive pixel in the detector and every angular step of the turn-table, the measured intensity is given by the Beer-Lambert law:

$$I = I_0 \cdot \exp\left(- \int_{\text{ray path}} \mu(x)dx \right) \quad (1)$$

where $\mu(x)$ stands for the attenuation coefficient along the ray path inside the inspected material. Measuring I and I_0 with the imaging device, we are then able to determine the integral of $\mu(x)$ along a great number of paths. This set of integrals is known as the Radon transform of the μ map of the object. Provided the Radon transform is reasonably well sampled, the projection-slice theorem allows the resolution of the inverse problem, i.e., the establishment of the μ map. In our case, image reconstruction is achieved using the three-dimensional FBP (filtered back-projection) algorithm of Feldkamp [12,13]. The computed μ values are correlated to the local density and chemical composition of the investigated specimen.

In this study, we used the scanner conceived and constructed at CNDRI, which allows high resolution 3D imaging of the internal structure of the material. The scanner (Fig. 1) mainly consists in a micro-focus X-ray tube (Philips 161 HOMX) and an X-ray sensitive camera. The small size of the X-ray tube focus allows geometrical magnification of the image, while maintaining a low value of the image blurring. The effective voxel size within the reconstructed image can be chosen between 15 and 100 μm. The imaging device, a low noise CCD camera, cooled by a triple-stage Peltier cooler and equipped with a high-aperture lens, is used to catch the weak visible image emitted by a terbium-doped Gd_2O_2S fluorescent screen.

A voxel size of 40 μm was selected for the reconstructed images of those specimens. The corresponding 3D image format ($700\times700\times400$ voxels) is thus able to completely describe a concrete specimen with dimensions of the section up to 30×30 mm^2 Due to the relatively low density of this kind of concrete, a 80 kV value of the X-ray tube potential was chosen. A copper filter, 0.2 mm in thickness, was directly set at the tube window, allowing the selective absorption of the lower energy components of the spectrum in order to reduce the "beam-hardening" artefacts [11]. Using a tube current of 0.1 mA, the overall acquisition and readout time for each of the 900 projections was 20 s (five hours for the scan). An example of 3D image is presented in Fig. 2.

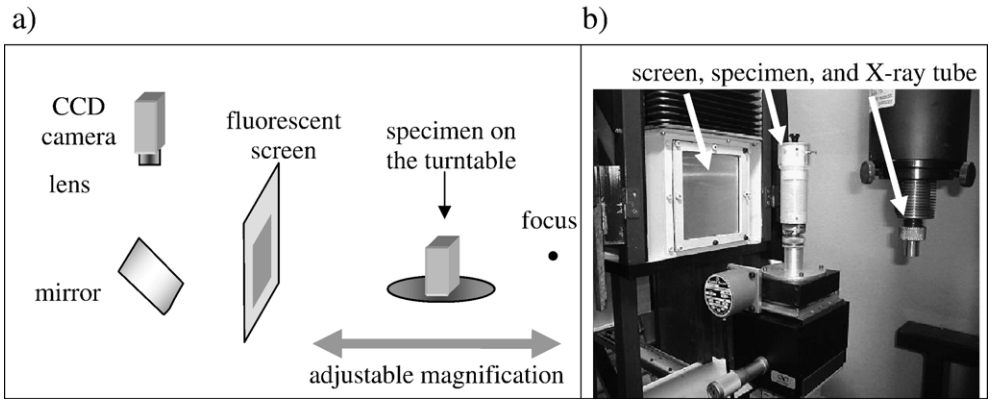

Fig. 1. Microtomography equipement, (a) general scheme, (b) photo of the device.

Fig. 3 shows cross sections of two specimens with bimodal EPS size distribution and respectively 492 and 961 kg/m^3 density, which have been extracted from 3D images. In high density specimens (Fig. 3b), two phases clearly appear, the cement in grey and EPS spheres in white. In low density specimens (Fig. 3a), it can also be observed white pores with a complex shape, which have been introduced during blending. The EPS spheres were extracted from the 3D images by a sequence of image processing operations: automatic thresholding algorithm based on dynamic clouds [14], objects segmentation and labelling using a watersheds-like algorithm [15] to separate the convex parts using Danielsson vector distance [16], and rejection of non spherical objects using a sphericity criterion. The image of EPS spheres can then be reconstructed from the obtained set of centres and radii. An example of EPS sphere extraction is presented in Fig. 4.

4. Determination of thermal and mechanical properties

The thermal conductivity of each material has been measured by using the Hot Wire method. This transient method is based on the measurement of the temperature increase at a defined distance from a linear heat source (hot wire) embedded in the tested material [17,18]. For each material, three specimens have been measured. Table 1 presents the average values of thermal conductivity. As expected, the conductivity is increasing with increasing density. Values between 0.13 and 0.45 W m^{-1} K^{-1} have been found.

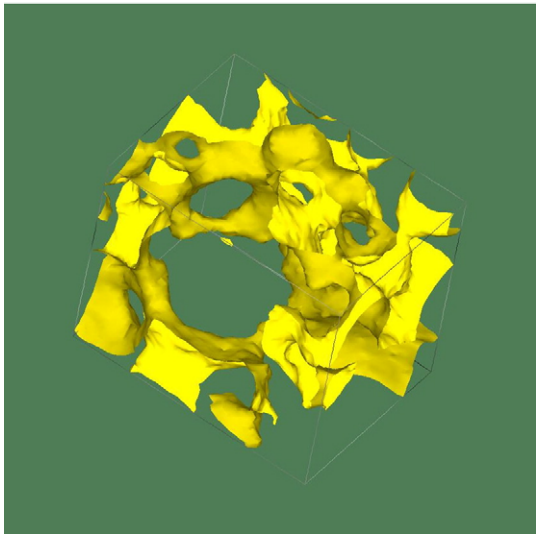

Fig. 2. 3D image of concrete matrix surrounding the (transparent) hole corresponding to an EPS sphere.

Compressive tests with constant displacement rate of 5 mm/min have been performed to characterize mechanical properties of EPS concretes. A typical stress–strain curve is shown on Fig. 5. Three parts can be distinguished: an initial part with a slow increase of stress, which includes the deformation of the loading device; a quasi linear part and a drop, which indicates specimen failure. The yield stress corresponding to the end of the elastic linear portion is difficult to estimate. Only the maximal stress will thus be considered and called compressive strength. For each density, 3 tests have been performed and the average compressive strength values has been calculated (Table 1). The strength is roughly correlated with the density. It varies between 0.03 for low density and 11.4 MPa for high density.

A summary of thermal and mechanical properties measurement is presented in Fig. 6 where the compressive strength is plotted *vs.* the thermal conductivity. This representation is particularly useful to compare the main features of EPS concretes with regard to other lightweight concretes. As an example typical properties of autoclaved cellular concrete are shown. It is observed that the lightest EPS concretes of density around 450 kg/m^3 has about the same conductivity as autoclaved cellular concrete but a much lower mechanical resistance. This result can be related with microstructure differences between both types of materials arising from their fabrication process: the autoclaved cellular concrete shows a higher strength because the pores are mostly isolated, spherical and smaller than the ones in the lightest EPS concrete. It can also be noted that there is no clear effect of EPS sphere size distribution in the properties shown in Fig. 6.

5. Modelling of thermal properties

Thermal properties of multiphase materials are quite well predicted by popular effective medium approaches including

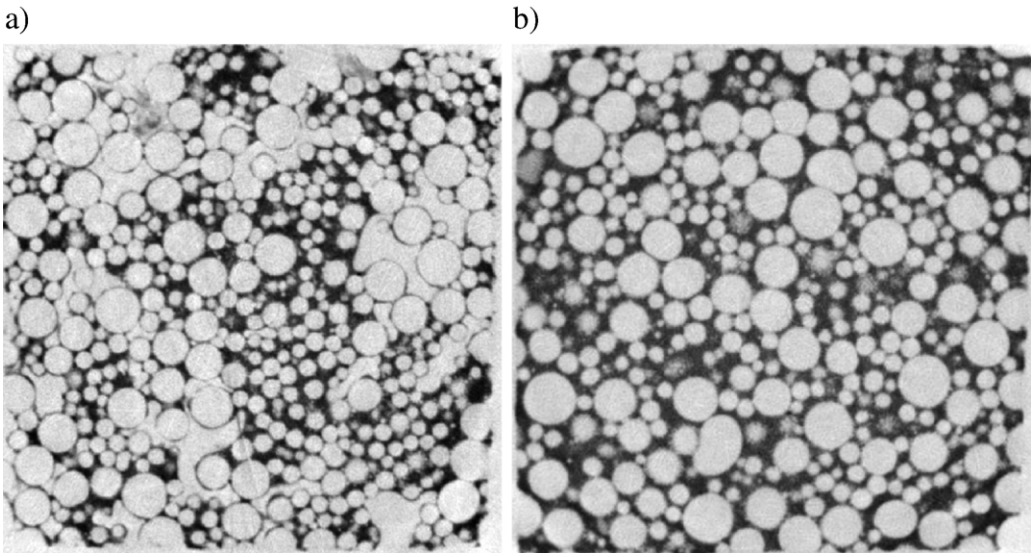

Fig. 3. Cross section of specimens of mass density 492 kg/m^3 (a) and 961 kg/m^3 (b) extracted from microtomography images.

self-consistent or differential approximations. In the present case, the material is supposed to be composed of two phases, a high conduction phase 1 comprising the cement matrix and a low conduction phase 2 including EPS spheres and porosity. If we neglect the mass of EPS spheres with regard to the mass of concrete, the volume fraction of conductive phase, $c_1=1-c_2$, can be considered as the relative density of the material, ϕ. The conductivity k_1 of the cement matrix is about unity whereas the conductivity of air is $k_2=0.025$ Wm^{-1}K^{-1}. The ratio k_2/k_1 is then equal to 1/40. Let us assume, in a first guess, that this ratio is zero, i.e., we consider the simplified case of perfectly isolated inclusions embedded in a conductive matrix. We can use the very simple scaling law derived by Gibson and Ashby [18] for cellular materials, to say $\frac{k^{\text{eff}}}{k_1} = C\phi$, where k^{eff} is the conductivity of the composite and $C=2/3$ for a closed-cell structure. In the following, the conductivity of air is taken into account.

A first relation is given by Maxwell's approximation [19]:

$$\frac{k^{\text{eff}}}{k_1} = 1 + \frac{1-\phi}{\frac{k_1}{k_2-k_1} + \frac{\phi}{3}} \tag{2}$$

It offers a good estimate of the conductivity of composites, provided that the inclusions of phase 2 are well separated from each other. In fact, Maxwell's approximation coincides with the well known Hashin & Shtrikman upper bound dedicated to isotropic composites. The implicit topological hypothesis is that the phase 2 is never percolating, even at very low values of relative density.

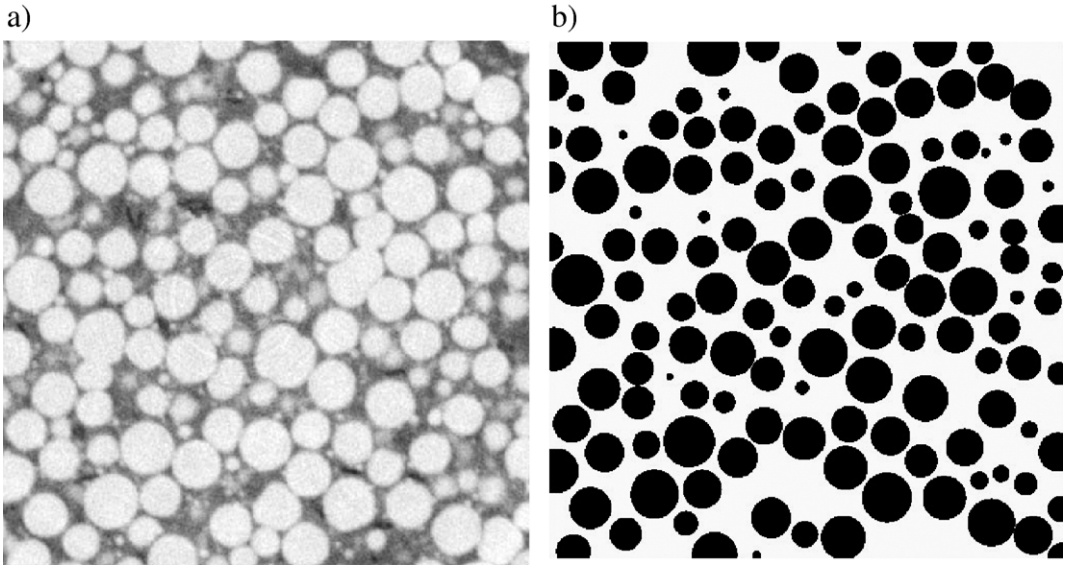

Fig. 4. Cross sections of the original 3D image (a) and of the reconstructed spheres (b) for material 8.

Table 1
Results of thermal and mechanical tests

Material #	EPS size distribution	Mass density (kg/m3)	Thermal conductivity (W m^{-1} kg^{-1})	Compressive strength (MPa)
1	Bimodal	492	0.164	0.8
2	Bimodal	615	0.206	2.5
3	Bimodal	705	0.238	4.2
4	Bimodal	817	0.250	7.4
5	Bimodal	961	0.300	9.2
6	Monosize	432	0.134	0.4
7	Monosize	630	0.219	2.3
8	Monosize	861	0.314	11.4

The differential effective medium (DEM) estimate introduced by Bruggeman [20] requires integrating the following differential equation with increasing volume fraction of second phase c_2:

$$\frac{dk^{\text{eff}}}{dc_2} = \frac{3k^{\text{eff}}}{(1-c_2)}\left[\frac{k_2 - k^{\text{eff}}}{k_2 + 2k^{\text{eff}}}\right]$$

with the initial condition $k^{\text{eff}}(c_2 = 0) = k_1$. (3)

The implicit topological hypothesis of this scheme is that the matrix phase 1 remains connected whatever the volume fraction c_1 is. Therefore, at low volume fraction, the DEM estimate corresponds to an open-cell structure whereas the Maxwell's estimate corresponds to a closed-cell structure.

The solution of Eq. (3) is also known as asymmetric Bruggeman's estimate. The symmetric Bruggeman's approximation corresponds to the so-called self consistent approach and is the positive root of the following second order equation:

$$2\left(\frac{k^{\text{eff}}}{k_1}\right)^2 - \left(\left(2 - \frac{k_2}{k_1}\right)\phi + \left(2\frac{k_2}{k_1} - 1\right)(1-\phi)\right) \times \left(\frac{k^{\text{eff}}}{k_1}\right) - \frac{k_2}{k_1} = 0 \quad (4)$$

In such a scheme, phases 1 and 2 play a symmetric role, which is not the case for the present material.

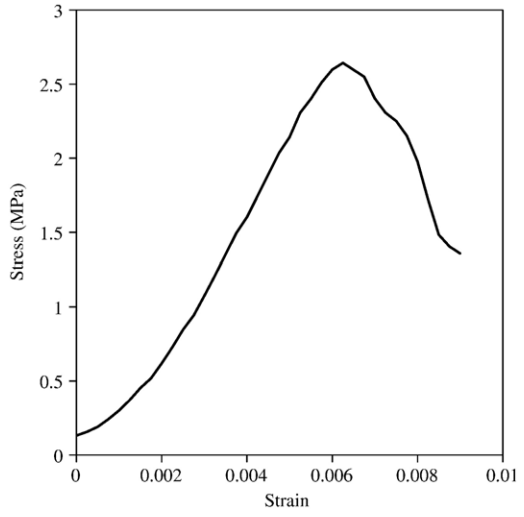

Fig. 5. Typical stress–strain curve obtained during compression of 615 kg/m^3 dense specimen.

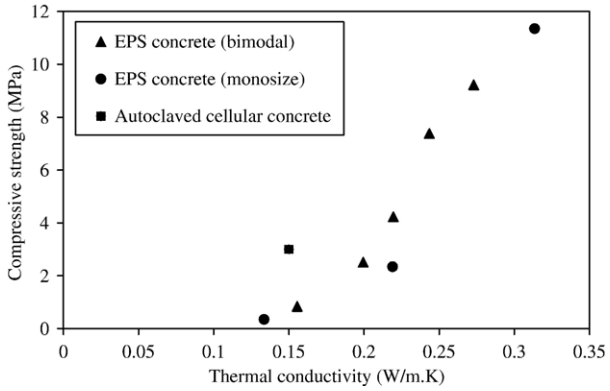

Fig. 6. Compressive strength vs. thermal conductivity for EPS concretes. Comparison with autoclaved cellular concrete.

Fig. 7 presents the experimental data obtained on EPS concrete in terms of relative conductivity (conductivity of EPS concrete divided by conductivity of cement) *vs.* relative density (density of EPS concrete divided by density of cement, the mass of EPS spheres being neglected) and compares them with the prediction of these three models. In the studied range of volume fraction, the best agreement is obtained with asymmetric Bruggeman's model, which is reasonable with regard to the basis of this model.

6. Modelling of mechanical properties

Stiffness and strength of EPS beads are negligible in comparison with the intrinsic properties of the cement matrix. From a mechanical point of view, EPS concretes can then be considered as cellular materials. Therefore it is relevant to address the modelling of their properties by referring to classical Gibson & Ashby's model [18]. This model predicts a power relation between the yield stress and the density with an exponent depending on whether the material comprises open or close cells.

The results of mechanical tests performed on EPS concretes are presented in Fig. 8 as the relative strength (strength of EPS concrete, σ_s, divided by strength of cement, σ_1) *vs.* the relative

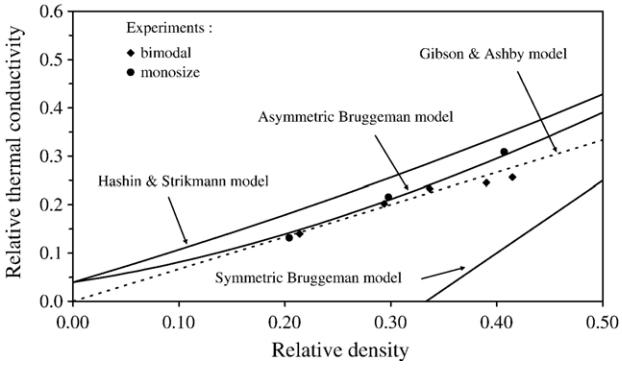

Fig. 7. Comparison of thermal conductivity predicted by various models with experimental data.

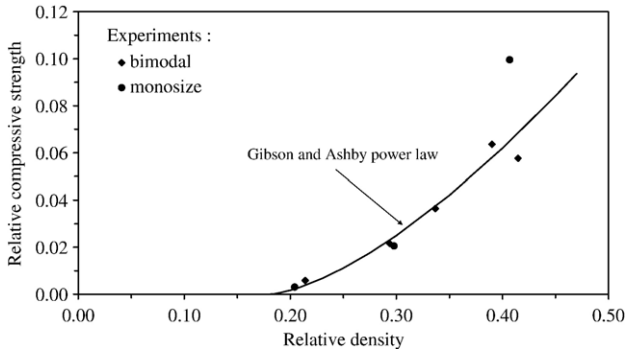

Fig. 8. Results of compression tests in terms of relative parameter. Adjustment with Gibson and Ashby power law (Eq. (5)).

density. They suggest that no strength is measurable for specimen with a relative density lower than 20%. It means that there is a mechanical percolation threshold. Introducing the threshold value for randomly packed monosized spheres [21], ϕ_c=0.18, allows fitting the experimental results by the following scaling law:

$$\frac{\sigma_s}{\sigma_1} \propto (\phi - \phi_c)^{1.5} \quad (5)$$

The exponent of this expression refers to a mechanism of deformation arising preferentially in the cell edges and not in the cell faces and corresponding thus to open cell cellular structures [18].

Such scaling laws derive from dimensional analysis. They predict the effect of the relative density but they are not able to take into account microstructural effects linked to the complexity of the cellular architecture. It is also the case of most mean field type methods. Another solution consists in the direct modelling of the microstructure provided by 3D images. The appropriate numerical tool to use in such complex situation is the Finite Element Method (FEM). It has been applied with success either to tomographic images of real materials or to numerically designed structures [22,23]. Generally the method lies in a straightforward transcription of the voxel structure of a three-dimensional image into a mesh of cubic elements, each voxel becoming an element. It often leads to solving very large systems, even for cellular materials. Sub-resolution technique, consisting in replacing a group of eight voxels by only one voxel, is a solution to overcome this limitation. It can lead however to a dramatic loss of information especially in the case of low relative density.

We have tested here another procedure based on the description of the microstructure from the above defined sets of spheres (radii and centres). From these data, it is possible to construct a tessellation of the space based on radical planes [24,25]: separation planes between two spheres are defined as the radical planes, i.e., points of equal tangency to the two spheres. When performing this construction for each pair of spheres, polyhedral convex cells are generated as illustrated in Fig. 9. This construction generalizes for spheres of different radii the classical Voronoi tessellation.

It has been previously deduced from relation (4) that EPS concretes can be schematized as open-cell structures at least from a mechanical point of view. We have then considered the tessellations issued from the image analysis, focusing only on the edges, i.e. transforming each edge into classical beam elements. The relative density was adjusted by changing beam thickness, which was supposed to be the same for all beams. Finite element calculations on such beam structures allowed determining the stress–strain curve during simple compression. We defined the yield strength as the stress resulting in the first beam failure within the structure. It does not necessarily correspond to the collapse of the structure. Therefore it cannot directly be compared with the compressive strength deduced from mechanical tests, which was defined as the maximum of the stress–strain curve. However we will assume in the following that both effective stress and compressive strengths show similar trends as function of microstructural features.

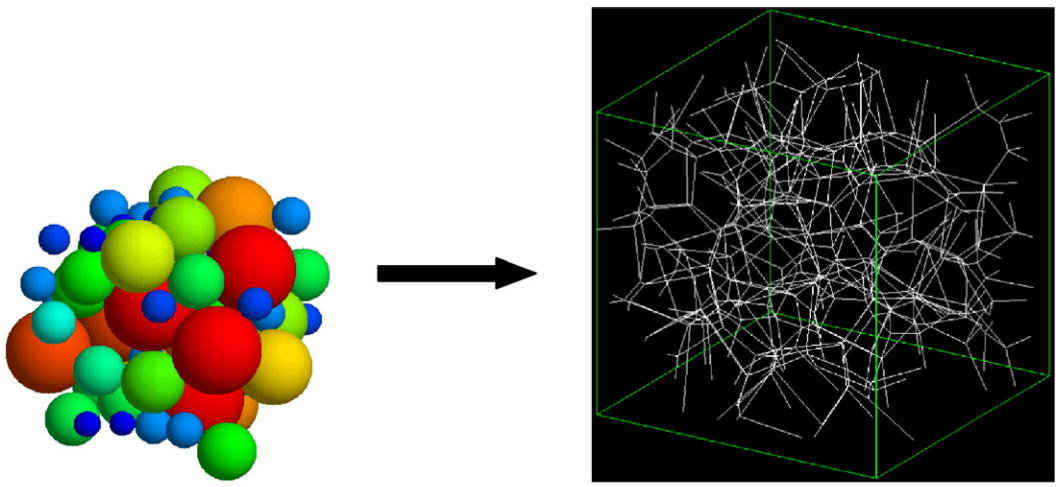

Fig. 9. Packing of spheres and corresponding structure obtained with the radical plane construction.

We have performed such a modelling procedure for materials 2 (ϕ=0.29) and 4 (ϕ=0.41). The following result was found:

$$\frac{\sigma_y(\phi = 0.41)}{\sigma_y(\phi = 0.29)} = 2.3 \quad (6)$$

whereas experimental data provide:

$$\frac{\sigma_c(\phi = 0.41)}{\sigma_c(\phi = 0.29)} = 2.6 \quad (7)$$

Hence the numerical simulation leads to a reasonable agreement with the experimental results.

7. Discussion and conclusion

Microstructural, mechanical and thermal features of EPS concretes with various densities have been characterized. Images obtained by microtomography showed three phases, EPS beads, cement and, in the lightest materials, pores with complex shapes. It has been found that the thermal conductivity was well described by asymmetric Bruggeman's model whereas the compressive strength followed Gibson and Ashby power law. Consistently, both models correspond to open-cell structures. From this set of information, it is possible to analyze whether EPS concretes can reach suitable thermal and mechanical characteristics simultaneously.

We choose the properties of autoclaved cellular concrete (ACC) as a reference for this discussion. ACC thermal conductivity is about 0.15 W m^{-1} K^{-1}. According to Bruggeman's model the conductivity of EPS concrete is smaller than this value when its relative density is lower than 0.25. ACC compressive strength is about 3 MPa. According to Gibson and Ashby relation fitted to our experimental data, the strength of EPS concrete is higher than this value when its relative density is higher than 0.3. Both requirements are thus incompatible. The condition associated with thermal conductivity seems to be necessary because the conductivity appeared to be essentially related to the volume fraction of conductive phase, i.e., to the relative density, and thus independent of the morphology of the insulating phase, provided that the assumption of open cell structure is verified. Therefore the efforts should be focused on increasing the mechanical resistance of low density concretes, which seems to be a more versatile parameter. Two tracks can be followed for this purpose. Of course, increasing the strength of the cement would lead to a proportional increase in concrete strength. The second solution consists in modifying the microstructure of the concrete for example by changing the particle size distribution of EPS beads. A wider distribution should lead to a closer packing and thus, for a given relative density, to a lower fraction of pores. As it is likely that pores are detrimental to the strength of the material, we can therefore expect an increase in strength. Also calculations of 2D beam structures generated from bimodal particle mixtures [26] showed significant variations in mechanical features when the particle size ratio was changed. Preliminary 3D simulations achieved with the procedure presented above indicated similar trends. This analysis should be pursued with a view to determining optimal EPS size distribution.

Even after such optimisation, it is unlikely that EPS concretes reach simultaneously the thermal and mechanical properties of ACC. EPS concretes can nevertheless be an interesting solution for the building industry as lightening component of a supportive structure, whose properties of this material can easily be tuned by changing its composition.

Acknowledgements

The authors thank Région Rhône-Alpes for its financial support to this work.

References

[1] D.J. Cook, Expanded polystyrene beads as lightweight aggregates for concrete, Precast Concrete 4 (1973) 691–693.
[2] B. Saaba, R.S. Ravindrarajah, Engineering properties of lightweight concrete containing crushed expanded polystyrene waste, Proc. Materials Research Society 1997 Fall Meeting, Boston, 1997.
[3] K.G. Babu, D.S. Babu, Behaviour of lightweight expanded polystyrene concrete containing silica fume, Cement and Concrete Research 33 (2003) 755–762.
[4] B. Chen, J. Liu, Properties of lightweight expanded polystyrene concrete reinforced with steel fiber, Cement and Concrete Research 34 (2004) 1259–1263.
[5] D.S. Babu, K.G. Babu, T.H. Wee, Properties of lightweight expanded polystyrene aggregate concretes fly ash, Cement and Concrete Research 35 (2005) 1218–1223.
[6] R. Le Roy, E. Parant, C. Boulay, Taking into account the inclusions' size in lightweight concrete compressive strength prediction, Cement and Concrete Research 35 (2005) 770–775.
[7] K. Miled, R. Le Roy, K. Sab, C. Boulay, Compressive behaviour of an idealized EPS lightweight concrete: size effects and failure mode, Mechanics of Materials 36 (2003) 1031–1046.
[8] C. Bonacina, M. Campanale, L. Moro, Analytical and experimental investigations on the heat transfer properties of light concrete, International Journal of Thermophysics 24 (2003) 1407–1414.
[9] F. Blanco, P. Garcia, P. Mateos, J. Ayala, Characteristics and properties of lightweight concrete manufactured with cenospheres, Cement and Concrete Research 30 (2000) 1715–1722.
[10] J. Baruchel, et al., X-ray Tomography in Material Science, Hermes-Science, Paris, 2000.
[11] P. Grangeat, La Tomographie, Hermes Science, Traité IC2, Paris, France, 2002.
[12] L.A. Feldkamp, L.C. Davis, J.W. Kress, Practical cone-beam algorithm, Journal of Optical Society 1 (1984) 612–619.
[13] A.C. Kak, M. Slaney, Principles of Computerized Tomographic Imaging, IEEE Press, New-York, 1988.
[14] E. Diday, Optimisation en classification automatique, INRIA Editions, Versailles, France, 1979.
[15] J. Serra, Image Analysis and Mathematical Morphology, Academic Press, 1982.
[16] P.E. Danielsson, Euclidean distance mapping, Computer Graphics and Image Processing 14 (1980) 227–248.
[17] H. Sallée, D. Quenard, Twin probes for measuring thermal conductivity and thermal effusivity, Proceedings of 14th European Conference on Thermophysical Propertie, September 16-19, 1996, Villeurbanne, France, 1996.
[18] L.J. Gibson, M.F. Ashby, Cellular Solids: Structure and Properties, 2nd edition, Cambridge University Press, Cambridge, UK, 1997.
[19] J.C. Maxwell, Treatise on Electricity and Magnetism, Clarendon Press, Oxford, 1873.
[20] D. Bruggeman, Berechnung verschiedener Physikalischer Konstanten von heterogenen Substanzen, Annalen der Physik (Liepzig) 24 (1935) 636–679.
[21] D. Bouvard, F.F. Lange, Relation between percolation and particle coordination in binary powder mixtures, Acta Metallurgica and Materialia 39 (1991) 3083–3090.

[22] A.P. Roberts, E.J. Garboczi, Elastic moduli of model random three-dimensional closed-cell cellular solids, Acta Materialia 49 (2001) 189–197.
[23] E. Maire, A. Fazekas, L. Salvo, R. Dendievel, S. Youssef, P. Cloetens, J.-M. Letang, X-ray tomography applied to characterization of cellular materials. Related finite element modelling problems, Composite Scence and Technology 63 (1997) 2431–2443.
[24] B.J. Gellatly, J.L. Finney, Characterisation of models of multicomponent amorphous metals: the radical alternative to the Voronoi polyhedron, Journal of Non-Crystalline Solids 50 (1982) 313–329.
[25] P. Richard, L. Oger, J.P. Troadec, A. Gervois, A tessellation of binary assemblies of spheres, Physica A 259 (1998) 205–221.
[26] A. Fazekas, R. Dendievel, L. Salvo, Y. Brechet, Geometrical effects on the stiffness and strength of 2D cellular structures, International Journal of Mechanical Sciences 44 (2002) 2047–2066.